Mesoporous $Ti_{0.5}Cr_{0.5}N$ Supported PdAg Nanoalloy as Highly Active and Stable Catalysts for the Electro-oxidation of Formic Acid and Methanol

Zhiming Cui, Minghui Yang, and Francis J. DiSalvo*

Department of Chemistry and Chemical Biology, Cornell University, Ithaca, New York 14850, United States

ABSTRACT We report a robust noncarbon $Ti_{0.5}Cr_{0.5}N$ support synthesized by an efficient solid–solid phase separation method. This ternary nitride exhibits highly porous, sintered, and random network structure with a crystallite size of 20–40 nm, resulting in a high specific surface area. It is not only kinetically stable in both acid and alkaline media, but also electrochemically stable in the potential range of fuel cell operation. Two typical anode reactions, formic acid oxidation in acid media and methanol oxidation in alkaline media, are employed to investigate the possibility of $Ti_{0.5}Cr_{0.5}N$ as an alternative to carbon. Bimetallic PdAg nanoparticles (~4 nm) act as anode catalysts for the two anode reactions. PdAg/$Ti_{0.5}Cr_{0.5}N$ exhibits much higher mass activity and durability for the two reactions than PdAg/C and Pd/C catalyst, suggesting that mesoporous $Ti_{0.5}Cr_{0.5}N$ is a very promising support in both acid and alkaline media.

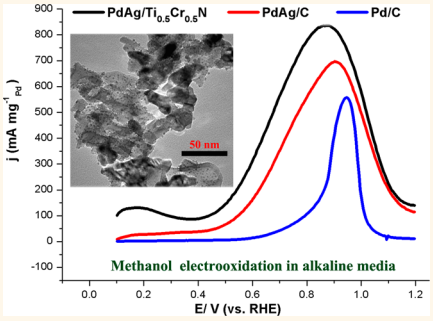

KEYWORDS: fuel cell · ternary nitride · PdAg alloy · methanol · formic acid

Fuel cells, especially polymer electrolyte membrane (PEM) fuel cells, are attractive alternatives to current energy conversion technologies due to their high power density, high efficiency and potentially zero emissions.[1,2] Despite recent advances, however, there are still several challenges that hinder fuel cell commercialization, including insufficient durability/reliability and high cost.[2,3] In terms of low durability of fuel cell catalysts, the corrosion of carbon support materials has been identified to be the major contributor to the catalyst failure. With the current state of technology, carbon black is the most practical support of catalysts for fuel cells. Unfortunately, carbon support is thermodynamically unstable in fuel cell environments due to its low equilibrium potential of 0.207 V relative to a reversible hydrogen electrode (RHE) at 25 °C.[2,4–7] For cathode catalysts, oxidation of the carbon support to CO_2 or CO can occur, resulting in the separation of Pt particles from the carbon support and loss of performance. In the case of anode catalyst, the carbon support can also be oxidized in the situation of fuel (hydrogen) starvation.[5,8] To address the issue of carbon support corrosion, some alternative support materials rather than the traditional carbon-based supporting materials should be explored.

For noncarbon support materials applied in fuel cells, some basic requirements should be met, including good conductivity (at least 0.1S/cm), high corrosion resistance, high surface area and high electrochemical stability under fuel cell operating conditions. Transition metal nitrides might be good alternatives due to their excellent conductivity, high hardness and high melting points.[6,9] Various nitrides including CrN and TiN have been explored for catalyst and catalyst support applications in fuel cells.[10–13] Most reports about nitrides as catalyst supports focus on simple binary nitrides, most often TiN. TiN has a number of desirable properties that make it uniquely suited as a potential replacement for carbon-based catalyst supports in fuel cells (in fact, TiN as a catalyst support was patented by General Motors in 2009). However, TiN suffers from wear and corrosion in highly acidic environments.[6,11,12] Therefore, TiN alone may not

* Address correspondence to fjd3@cornell.edu.

Received for review March 13, 2014 and accepted May 16, 2014.

Published online May 16, 2014
10.1021/nn5014337

possess the necessary stability to replace carbon-based supports. Recently we reported a ternary nitride ($Ti_{0.5}Nb_{0.5}N$) synthesized by a coprecipitation method.[14] This ternary nitride is chemically stable in acid media, which solves the TiN corrosion problem. However, its conductivity is much lower than that of the binary nitrides reported,[15,16] which may arise from the presence of K species in the surface passivation layer.[14] Therefore, it is desirable to further investigate other ternary nitrides and develop new synthesis strategy.

In this work, we report a robust noncarbon $Ti_{0.5}Cr_{0.5}N$ support with excellent electronic conductivity and high surface area synthesized by a solid−solid phase separation method. This ternary nitride is chemically stable in both acid media and alkaline media. Two typical anode reactions, formic acid oxidation in acid media and methanol oxidation in alkaline media, were employed to investigate this ternary nitride $Ti_{0.5}Cr_{0.5}N$. Regarding the electro-oxidation reactions of formic acid and methanol, the most common anode catalyst is Pt, but it is readily poisoned by strongly adsorbed intermediates like CO, resulting in poor catalytic activity.[17−22] Its high cost and limited resource are also the main blockages for commercialization of direct liquid fuel cells. Pd catalyst has been found to possess superior performances compared to Pt due to dominance of the direct dehydrogenation pathway.[23−26] But its activity is not stable, and periodic regeneration is required.[27−29] Pd has also been considered a promising catalyst toward methanol oxidation in alkaline media.[30,31] Alloying Pd with a second metal has been proved to be a successful strategy to further enhanced activity and stability for both formic acid oxidation in acid media and methanol oxidation in alkaline media.[32−39] Here, bimetallic PdAg nanoalloy was selected as the catalyst for the two anode reactions. Supported bimetallic PdAg catalysts were prepared by simultaneous reduction of silver and palladium precursors with $NaBH_4$ as reducing agent and $Ti_{0.5}Cr_{0.5}N$ (and carbon) as supports. The electrocatalytic behaviors of the nitride supported PdAg catalyst for the two anode reactions and were investigated and compared with PdAg/C and Pd/C catalysts, to show significant enhancement activity and stability of the new support-based catalyst.

RESULTS AND DISCUSSION

Mesoporous $Ti_{0.5}Cr_{0.5}N$ was prepared by a solid−solid phase separation method from a Zn containing metal oxides. Under a flow of ammonia gas at 800 °C, Zn^{2+} is reduced to Zn metal and sublimed out of Zn containing metal oxides; the oxide is reduced to form mesoporous $Ti_{0.5}Cr_{0.5}N$ as a free-flowing black powder. The morphology and structure of the mesoporous $Ti_{0.5}Cr_{0.5}N$ are characterized using scanning electron microscopy as shown in Figure 1a. $Ti_{0.5}Cr_{0.5}N$ exhibits highly porous, sintered and random network structure

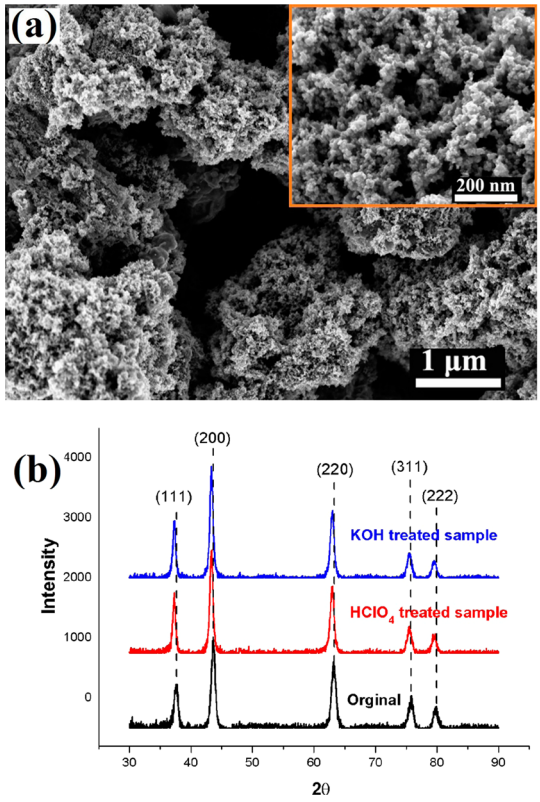

Figure 1. (a) Scanning electron microscopy images (SEM) of $Ti_{0.5}Cr_{0.5}N$; (b) XRD pattern of $Ti_{0.5}Cr_{0.5}N$ before and after chemical stability test.

with a crystallite size of 20−40 nm, resulting in high specific surface area. As shown in Figure S1 (Supporting Information), TiN also shows similar morphology and structure to $Ti_{0.5}Cr_{0.5}N$. Nitrogen physisorption measurements (Figure S2, Supporting Information) show that the BET surface areas of $Ti_{0.5}Cr_{0.5}N$ and TiN are 72 and 63 $m^2\ g^{-1}$, respectively. Electronic conductivity of supports plays a critical role in catalyst activity and is measured using a homemade 4-point probe.[14] This apparatus applied pressure to compacted powder while the electrical measurements were made. At 35 bar, the conductivities of $Ti_{0.5}Cr_{0.5}N$ and TiN are 68 and 90 S cm^{-1}, which are about 1 order of magnitude higher than the value we measured (1.5 S cm^{-1}) and the value reported (4 S cm^{-1}) for carbon black.[40] The atomic ratio of Ti/Cr ratio is 0.95, which is determined by energy dispersive X-ray spectra (EDX).

The phase purity of the product is confirmed by powder X-ray diffraction (pXRD) in Figure 1b. For as-prepared $Ti_{0.5}Cr_{0.5}N$, the diffraction peaks at 36.2°, 42.2°, 61.3°, 73.4° and 77.3° can be assigned to (111), (200), (220), (311), and (222) lattice planes of face-centered cubic $Ti_{0.5}Cr_{0.5}N$ (PDF#04−016−6620). To investigate the chemical stability of nitrides in acid media, $Ti_{0.5}Cr_{0.5}N$ and TiN are soaked in 0.1 M $HClO_4$ solution for two months. For $Ti_{0.5}Cr_{0.5}N$ sample after stability tests in acid media, there are no observable changes in the XRD pattern before and after stability

test, and the $Ti_{0.5}Cr_{0.5}N$ remains black (Figure S3, Supporting Information) indicating that the material is chemically stable. $Ti_{0.5}Cr_{0.5}N$ is also chemically stable in alkaline media after soaked in 0.1 M KOH solution for two months. In the case of as-prepared TiN, the XRD pattern in Figure S4a (Supporting Information) display the (111), (200), (220), (311), and (222) reflections, confirming the face-centered cubic structures of TiN (PDF#65−0715). TiN partially becomes TiO_2 (PDF#65−1119) after soaking in 0.1 M $HClO_4$ solution for two months, while TiN is chemically stable after soaking in 0.1 M KOH solution, which is seen in Figure S4 (Supporting Information). Figure S5 (Supporting Information) shows the results of TGA measurements performed in air for $Ti_{0.5}Cr_{0.5}N$. Oxidation begins at above 200 °C, which means that $Ti_{0.5}Cr_{0.5}N$ is "stable" in air below ~200 °C.

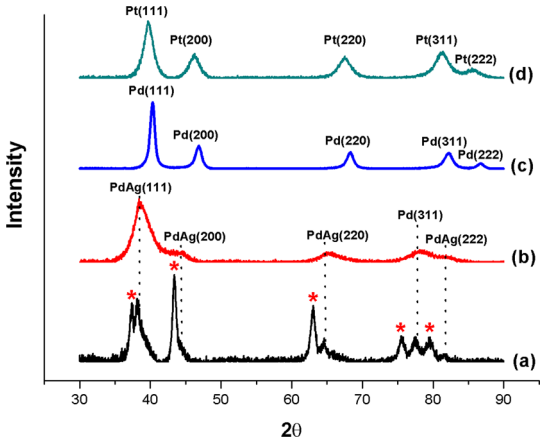

Figure 2. XRD patterns of (a) PdAg/$Ti_{0.5}Cr_{0.5}N$, (b) PdAg/C, (c) Pd/C, and (d) Pt/C. The peak positions of $Ti_{0.5}Cr_{0.5}N$ are marked with *.

PdAg nanoparticles were deposited on $Ti_{0.5}Cr_{0.5}N$ using an impregnation method with sodium borohydride as reducing agent.[41] For comparison, PdAg/, Pd/C and Pt/C were also prepared through the same process. The XRD patterns for PdAg/$Ti_{0.5}Cr_{0.5}N$, PdAg/C, Pd/C and Pt/C are shown in Figure 2a,b,c,d. All the diffraction peaks of $Ti_{0.5}Cr_{0.5}N$ are observed in PdAg/$Ti_{0.5}Cr_{0.5}N$ catalyst. The PdAg particles crystallize in space group $Fm\bar{3}m$ (225) with refined lattice parameter a = 4.029 Å (PDF#01−080−4045). For PdAg/C, the diffraction peaks of PdAg are almost identical to those of PdAg on mesoporous $Ti_{0.5}Cr_{0.5}N$. For Pd/C, Pd particles crystallize in space group $Fm\bar{3}m$ with refined lattice parameter a = 3.891 Å. The actual metal loading in PdAg/$Ti_{0.5}Cr_{0.5}N$, PdAg/C, Pd/C and Pt/C are 20.3, 19.6, 19.4 and 20.1 wt %, respectively, which was analyzed by EDX. The atomic ratios of Pd/Ag in PdAg particle (randomly chosen) are 1.01 ± 0.2 for PdAg/$Ti_{0.5}Cr_{0.5}N$ and 0.98 ± 0.3 for PdAg/C, which are consistent with the Pd/Ag ratio in the precursor (with Pd-to-Ag mole ratio of 1). The corresponding loadings of Pd in PdAg/$Ti_{0.5}Cr_{0.5}N$ and PdAg/C are 10.2 and 9.5 wt %, respectively. TEM images of PdAg/$Ti_{0.5}Cr_{0.5}N$, PdAg/C, Pd/C and Pt/C are shown in Figure 3, and their corresponding histograms of metal nanoparticles are presented in Figure S6 (Supporting Information). Histograms of metal nanoparticle diameters were obtained by measuring the size of 200 particles in random regions. The average sizes of metal particles in the

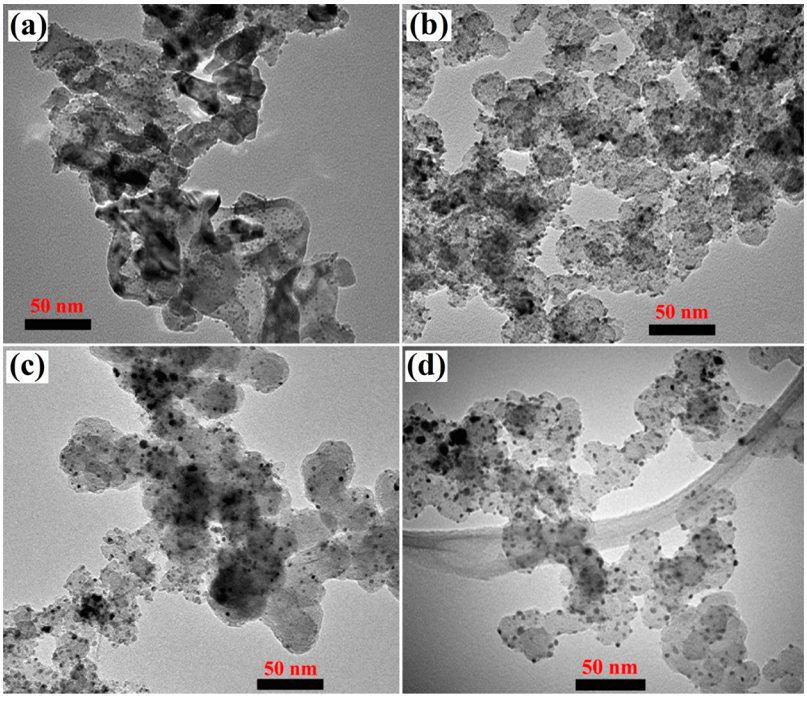

Figure 3. TEM images of (a) PdAg/$Ti_{0.5}Cr_{0.5}N$ catalyst, (b) PdAg/C catalyst, (c) Pd/C catalyst, and (d) Pt/C catalyst.

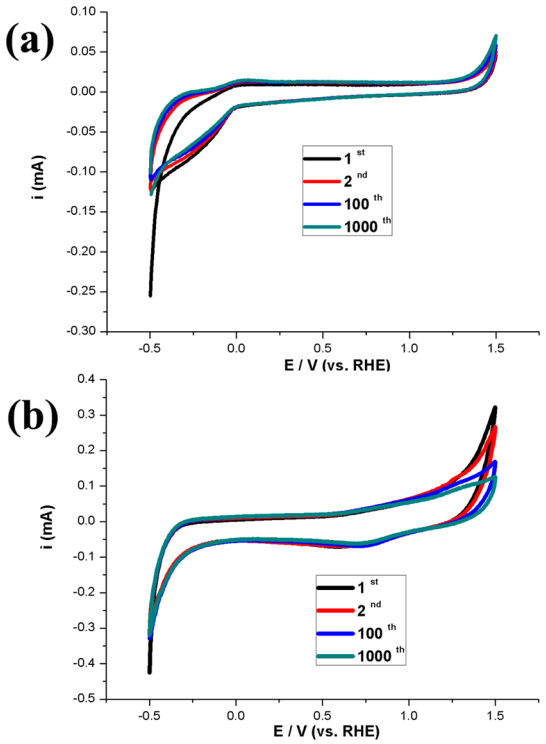

Figure 4. (a) Cyclic voltammograms of $Ti_{0.5}Cr_{0.5}N$ in 0.1 M $HClO_4$ solution. (b) Cyclic voltammograms of $Ti_{0.5}Cr_{0.5}N$ in 0.1 M KOH solution.

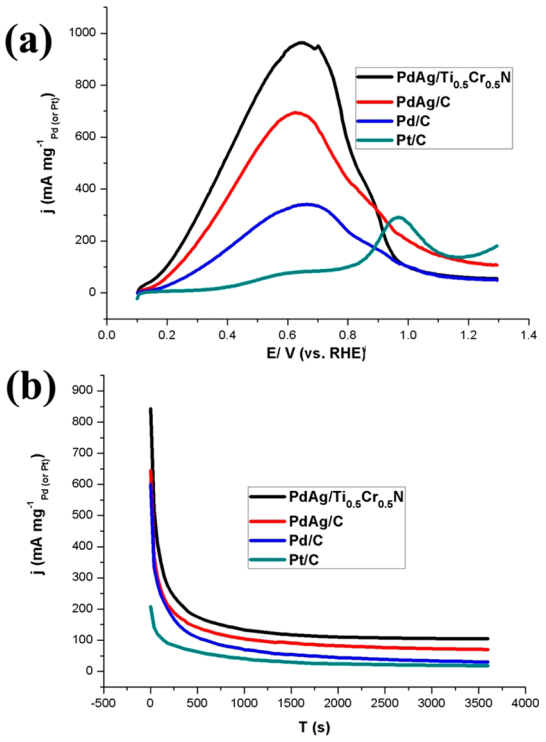

Figure 5. (a) Linear sweep voltammograms of the catalyst samples performed in electrolytes of 0.1 M $HClO_4$ + 1 M HCOOH at a scan rate of 10 mV s^{-1}. (b) Polarization current *vs* time plots of four kinds of catalysts electrodes measured in 0.1 M $HClO_4$ + 1 M HCOOH solution.

$PdAg/Ti_{0.5}Cr_{0.5}N$, PdAg/C, Pd/C and Pt/C catalysts as estimated from their histograms are 3.9 ± 0.4, 4.2 ± 0.5, 5.7 ± 0.6 and 4.8 ± 0.5 nm, respectively. More TEM images of $PdAg/Ti_{0.5}Cr_{0.5}N$ are presented in Figure S7 (Supporting Information). PdAg particles supported on $Ti_{0.5}Cr_{0.5}N$ support are smaller and more uniformly dispersed than those on carbon, thus indicating that supports play an important role in dispersion and growth of PdAg particles. Pd nanoparticles in Pd/C catalyst has wide size distribution with some large particles, obviously caused by serious aggregations.

The electrochemical stability of $Ti_{0.5}Cr_{0.5}N$ powder is examined under applied potential conditions comparable to those of a fuel cell. The sample was tested over a potential range from −0.5 to +1.5 V (*vs* RHE) in 0.1 M $HClO_4$ and 0.1 M KOH solutions at room temperature. As shown in Figure 4a, the nitride is not electrochemically active in the potential range of fuel cell operation (0 to +1.2 V *vs* RHE) in acid media, suggesting a stable surface. Moreover, when cycling repeatedly between those potentials for 1000 cycles, there is no sign of redox peaks associated with $Ti_{0.5}Cr_{0.5}N$, indicating that $Ti_{0.5}Cr_{0.5}N$ is electrochemically stable. The large current density below 0 V may be attributed to the hydrogen evolution. Similar to its electrochemical behavior in acid media, $Ti_{0.5}Cr_{0.5}N$ is also electrochemically stable in alkaline media, as shown in Figure 4b. The electrochemical stability is also confirmed TEM as shown in Figure S8 (Supporting Information). There are no observable changes in morphology before and after 1000 cycles in both acid and alkaline media.

Figure 5a is the linear sweep voltammograms (LSV) performed in a 0.1 $HClO_4$ solution +1 M HCOOH solution. The onset potential on $PdAg/Ti_{0.5}Cr_{0.5}N$ (0.15 V) is more negative than those on PdAg/C (0.16 V) and Pd/C (0.17 V), indicating that the formic acid is easier to be oxidized on $PdAg/Ti_{0.5}Cr_{0.5}N$. The peak current density for $PdAg/Ti_{0.5}Cr_{0.5}N$ is 975 mA mg^{-1}_{Pd}, which is ∼1.5 and 2.8 times higher than those for PdAg/C (670 mA mg^{-1}_{Pd}), and Pd/C (344 mA mg^{-1}_{Pd}). The LSV curves on three supported Pd-based catalysts toward formic acid oxidation show a prominent current peak at 0.5−0.6 V (*vs* RHE) and a shoulder one at ∼0.9 V (*vs* RHE), displaying an electrochemical behavior toward HCOOH oxidation similar to the Pt/C catalyst. The oxidation of formic acid on Pt involves a dual path mechanism, a dehydrogenation path to the direct formation of CO_2 and a dissociative adsorption to form poisoning CO species by a dehydration path.[42,43] Thus, it is reasonable to assign the first peak for supported Pd catalysts to a dehydrogenation path while the second peak is related to a dehydration path as specified for the Pt/C catalyst.[5,35] One could note that the onset potential for the second peak is similar to that of CO_{ad} oxidation, further proving that the second peak is indeed related to the oxidation of adsorbed CO or CO-like intermediate, that has been proved by surface-enhanced infrared

absorption spectroscopy.[44] The ratio of the first peak current to the second peak current could give an indication of which is the main reaction path.[20] The ratios for PdAg/$Ti_{0.5}Cr_{0.5}N$ (4.4) is much higher than those for PdAg/C (3.2) and Pd/C (2.9), suggesting that PdAg/$Ti_{0.5}Cr_{0.5}N$ significantly enhance the dehydrogenation path and diminish the poisoning of the catalysts.

The long-term stability of these catalysts is evaluated by chronoamperometry curves as shown in Figure 5b. The polarization current for the formic acid oxidation reaction on these three supported Pd-based catalysts shows a significant decay initially and reaches a stable value after polarized at 0.6 V (*vs* RHE) for ~700 to 900 s. The current decay for the HCOOH oxidation reaction indicates the slow deactivation of supported Pd-based electrocatalysts by slow adsorption of CO or CO-like intermediates.[28,45] However, the stable mass specific current for formic acid oxidation reaction on PdAg/$Ti_{0.5}Cr_{0.5}N$ is ~106 mA mg^{-1}_{Pd}, which is significantly higher than PdAg/C (~70 mA mg^{-1}_{Pd}) and Pd/C (~31 mA mg^{-1}_{Pd}). This indicates that PdAg/$Ti_{0.5}Cr_{0.5}N$ catalysts possess much better stability against the poisoning by adsorbed CO or CO-like intermediate species. The stability of the catalysts was also assessed by applying potential between 0.2 and 0.8 V (RHE) in 0.1 M $HClO_4$ + 1 M HCOOH solution at 100 mV s^{-1}. The linear sweep voltammograms of PdAg/$Ti_{0.5}Cr_{0.5}N$, PdAg/C and Pd/C catalysts after stability tests of 1000 cycles is presented in Figure S9 (Supporting Information). The peak current densities on PdAg/$Ti_{0.5}Cr_{0.5}N$ is reduced by 54.6%, which is lower than the reduction on PdAg/C (63.7%) and Pd/C (74.2%), further confirming that PdAg/$Ti_{0.5}Cr_{0.5}N$ exhibits the higher catalytic stability and is in good agreement with the result of chronoamperometry curves.

The methanol oxidation reaction in alkaline media is a reaction of interest for alkaline direct methanol fuel cells. Methanol oxidation in alkaline media is faster than in the presence of acidic electrolytes. Thus, from a kinetic viewpoint, it is advantageous to carry out methanol oxidation in alkaline electrolytes.[46] Figure 6a displays the linear sweep voltammograms of methanol electro-oxidation in electrolytes of 0.1 M KOH + 1 M CH_3OH. The onset potentials for PdAg/$Ti_{0.5}Cr_{0.5}N$ and PdAg/C are similar to that on Pt/C, but 0.3 V more negative than that on Pd/C. The peak current densities for PdAg/$Ti_{0.5}Cr_{0.5}N$ and PdAg/C are 844 and 717 mA mg^{-1}_{Pd}, which are ~1.5 and ~1.3 times higher than that for Pd/C (551 mA mg^{-1}_{Pd}). The onset oxidation potential, peak potential and current density are given in Table 1, demonstrating that the Ag/$Ti_{0.5}Cr_{0.5}N$ and PdAg/C have much higher activity toward methanol oxidation in alkaline media than Pd/C. Figure 6b shows the chronoamperometry curves for methanol oxidation on the PdAg/$Ti_{0.5}Cr_{0.5}N$, PdAg/C, Pd/C and Pt/C catalysts at a potential of 0.9 V (*vs* RHE). The stable

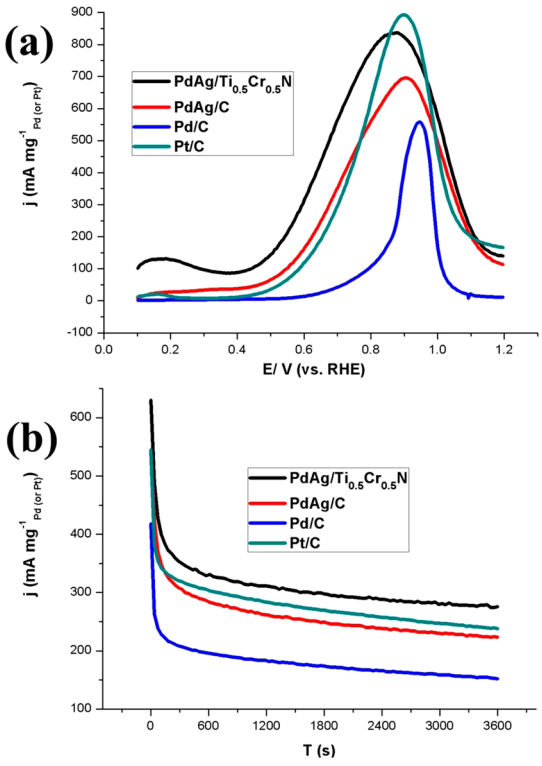

Figure 6. (a) Linear sweep voltammograms of the catalyst samples performed in electrolytes of 0.1 M KOH + 1 M CH_3OH at a scan rate of 10 mV s^{-1}. (b) Polarization current *vs* time plots of four kinds of catalysts electrodes measured in KOH + 1 M CH_3OH solution.

TABLE 1. Onset Potential, Peak Potential and Peak Current Density of PdAg/$Ti_{0.5}Cr_{0.5}N$, PdAg/C, Pd/C and Pt/C Catalysts for Methanol Oxidation in Alkaline Media

sample	onset potential (V)	peak current potential (V)	peak current density (mA mg^{-1}_{Pd})
PdAg/$Ti_{0.5}Cr_{0.5}N$	0.4	0.87	844
PdAg/C	0.43	0.90	717
Pd/C	0.45	0.95	551
Pt/C	0.7	0.89	896[a]

[a] mA mg^{-1}_{Pt}

current densities for methanol oxidation on PdAg/$Ti_{0.5}Cr_{0.5}N$, PdAg/C, Pd/C and Pt/C catalysts are ~292, 261, 246, 157 mA mg^{-1}_{Pd}, respectively. Among these four catalysts, PdAg/$Ti_{0.5}Cr_{0.5}N$ exhibits the highest stable current density, suggesting that PdAg/$Ti_{0.5}Cr_{0.5}N$ catalysts possess best electrocatalytic activity and stability toward methanol oxidation in alkaline media. This result is also confirmed by cyclic voltammetric method by applying potential between 0.5 and 1 V (RHE) in 0.1 M KOH + 1 M methanol solution at 100 mV s^{-1}. After 1000 cycles, as shown in Figure S10 (Supporting Information), the peak current density on PdAg/$Ti_{0.5}Cr_{0.5}N$ is reduced by 34.1%, which is lower than the reduction on PdAg/C (37.8%), Pd/C (45.7%) and Pt/C (40.9%).

The PdAg/$Ti_{0.5}Cr_{0.5}N$ catalyst exhibits significant enhancement in the catalytic activity and stability toward formic acid and methanol oxidation as compared to PdAg/C and Pd/C catalysts, which apparently arises from Ag and $Ti_{0.5}Cr_{0.5}N$. According to d-band theory,[18,47−49] the trend of reactivity follows the d-band center values of overlayer and impurity atoms. If the d-band center is shifted up, the adsorption ability of the adsorbate onto the metals becomes stronger and may help to improve the electro-oxidation of alcohol on the surface of the metals. According to density functional calculations by Nørskov *et al.*, the d-band center of Pd is shifted up after combining with Ag.[18] In other words, Ag can promote the electro-oxidation of formic acid and methanol oxidation by changing the electronic properties of Pd. Additionally, compared to PdAg/C, PdAg/$Ti_{0.5}Cr_{0.5}N$ catalyst shows enhanced performance for formic acid and methanol oxidation, which apparently arises from excellent conductivity, good chemical and electrochemical stability of $Ti_{0.5}Cr_{0.5}N$.

CONCLUSIONS

We have developed a robust noncarbon $Ti_{0.5}Cr_{0.5}N$ support with excellent conductivity by an efficient solid−solid phase separation method. This ternary nitride is not only chemically stable in both acid media and alkaline media, but also electrochemically stable in the potential range of fuel cell operation. Compared to monometallic Pd, bimetallic PdAg exhibits significant enhancement in the catalytic activity and stability toward not only formic acid oxidation in acid media but also methanol oxidation in alkaline media, which may arise from electronic (ligand) effects. $Ti_{0.5}Cr_{0.5}N$ supported PdAg catalyst exhibits the highest activity and stability for formic acid oxidation in acid media and methanol oxidation in alkaline media, suggesting $Ti_{0.5}Cr_{0.5}N$ is a very promising support. The solid−solid phase separation approach could be potentially applied to rational design of other conducting, porous and chemically stable materials like ternary nitrides for technologies including but not limited to fuel cells, solar cells and batteries.

EXPERIMENTAL SECTION

Materials. ZnO (99.99%, Aldrich); Cr_2O_3 (99.99%, Aldrich); TiO_2 (99.995%, Puratronic from Alfa Aesar); ammonia gas (Anhydrous, Air Gas); Vulcan XC-72 carbon black (Cabot Corporation); $Pd(NO_3)_2 \cdot 2H_2O$ (99.0%, Sigma-Aldrich), $AgNO_3$ (99.0%, Sigma-Aldrich); $NaBH_4$ (99.99%, Sigma-Aldrich). Nylon-66 filter membranes (pore size 0.20 μm, diameter 47 mm, Sigma-Aldrich)

Mesoporous $Ti_{0.5}Cr_{0.5}N$ and TiN. $Ti_{0.5}Cr_{0.5}N$ and TiN were prepared by a solid−solid separation method as reported previously.[50] The solid solution of the Zn containing metal oxide precursors (ZMO) were first prepared by preheating the specific mixture of metal oxides of ZnO, Cr_2O_3 and TiO_2 at temperatures between 600 and 1350 °C followed by cooling at 300 °C/h. The $Ti_{0.5}Cr_{0.5}N$ was prepared by ammonolysis of about 0.5 g of ZMO in an alumina boat. The boat was then placed in a silica tube with airtight stainless steel end-caps that had welded valves and connections to input and output gas lines. All gases were purified to remove trace amounts of oxygen or water using pellet copper, nickel, palladium and platinum with zeolites as support. The silica tube was then placed in a split tube furnace and the appropriate connections to gas sources made. Argon gas was passed over the sample for 15 min to expel air before establishing a flow of ammonia gas (Anhydrous, Air Gas). The ZMO was heated to the 800 °C at a heating rate of 150 °C/h. The furnace power was turned off after 8 h and the product cooled to room temperature in ~4 h under an ammonia flow. Before the silica tube was taken out of the split tube furnace, argon gas was flowed through the tube to expel the ammonia gas. The silica tube was left in lab for 24 h with one valve open in order to expose the ammonolysis product to air slowly.

PdAg/$Ti_{0.5}Cr_{0.5}N$. First, 50 mg of mesoporous $Ti_{0.5}Cr_{0.5}N$ (or C) was suspended in 50 mL of deionized water and treated in an ultrasonic bath. 9.9 mg of $AgNO_3$ and 15.6 mg of $Pd(NO_3)_2 \cdot 2H_2O$ was added to the suspension above. With dropwise addition of 20 mL of $NaBH_4$ solution (0.2 M), Pd^{2+} and Ag^{+} were reduced to PdAg nanoparticles. Subsequently, the resulted suspension was filtered by Nylon-66 filter membranes and washed with deionized water, and then dried at 60 °C for 6 h to obtain the PdAg/$Ti_{0.5}Cr_{0.5}N$ catalysts (or PdAg/C)

Physicochemical Characterization. Finely ground powders were examined with a Rigaku Ultima VI powder X-ray diffractometer (PXRD) with CuK radiation ($K\alpha_1$, λ= 1.5406 Å and $K\alpha_2$, λ = 1.5444 Å). Crystal structures of the oxides and resultant nitrides were confirmed by PXRD profiles using GSAS. Scanning electron microscopy (SEM) and energy dispersive X-ray analysis (EDX) were performed with a LEO-1550 field emission SEM (FSEM). PdAg on mesoporous $Ti_{0.5}Cr_{0.5}N$ and Vulcan XC-72 carbon black were performed with a transmission electron microscopy (FEI T12 Spirit TEM STEM) at 120 kV. The samples for TEM were prepared by sonicating the powders in ethanol for 30 min following which 3.05 mm holey carbon copper grids were dipped into the solution and dried in air. Nitrogen adsorption/desorption isotherms were measured at −196 °C using a Micromeritics ASAP 2020 system. The samples were degassed at 200 °C for 24 h on a vacuum line.

Electrochemical Measurements. Electrochemical measurements were carried out with a potentiostat/galvanostat (WaveNano USB Potentiostat) and a conventional three-electrode test cell. The catalyst ink was prepared by ultrasonically dispersing the mixture of 5 mg of catalysts, 1 mL of ethanol, and 50 μL of 5 wt % Nafion solutions. 10 μL of catalyst inks was pipetted and spread on the glassy carbon disk. A Pt foil and silver−silver chloride electrode were used as the counter and reference electrodes, respectively.

Conflict of Interest: The authors declare no competing financial interest.

Acknowledgment. This work by Zhiming Cui (preparation and evaluation of reported catalysts) was supported by the Energy Materials Center at Cornell, an Energy Frontier Research Center funded by the U.S. Department of Energy, Office of Basic Energy Sciences under Award Number DE-SC0001086. The preparation of mesoporous nitride materials by Minghui Yang was supported by National Science Foundation through Grant DMF-0602526.

Supporting Information Available: SEM images of TiN; Isotherm plot of N_2 absorption of $Ti_{0.5}Cr_{0.5}N$ and TiN; Corrosion test of $Ti_{0.5}Cr_{0.5}N$ and TiN; Linear sweep voltammograms of the catalyst samples after stability tests; Cyclic voltammograms of the catalyst samples. This material is available free of charge *via* the Internet at http://pubs.acs.org.

REFERENCES AND NOTES

1. Arico, A. S.; Bruce, P.; Scrosati, B.; Tarascon, J. M.; Van Schalkwijk, W. Nanostructured Materials for Advanced Energy Conversion and Storage Devices. *Nat. Mater.* **2005**, *4*, 366–377.
2. Debe, M. K. Electrocatalyst Approaches and Challenges for Automotive Fuel Cells. *Nature* **2012**, *486*, 43–51.
3. Van, T. T. H.; Pan, C. J.; Rick, J.; Su, W. N.; Hwang, B. J. Nanostructured $Ti_{0.7}Mo_{0.3}O_2$ Support Enhances Electron Transfer to Pt: High-Performance Catalyst for Oxygen Reduction Reaction. *J. Am. Chem. Soc.* **2011**, *133*, 11716–11724.
4. Chen, J. X.; Siegel, J. B.; Matsuura, T.; Stefanopoulou, A. G. Carbon Corrosion in PEM Fuel Cell Dead-Ended Anode Operations. *J. Electrochem. Soc.* **2011**, *158*, B1164–B1174.
5. Franco, A. A.; Guinard, M.; Barthe, B.; Lemaire, O. Impact of Carbon Monoxide on PEFC Catalyst Carbon Support Degradation Under Current-cycled Operating Conditions. *Electrochim. Acta* **2009**, *54*, 5267–5279.
6. Wang, Y. J.; Wilkinson, D. P.; Zhang, J. J. Noncarbon Support Materials for Polymer Electrolyte Membrane Fuel Cell Electrocatalysts. *Chem. Rev.* **2011**, *111*, 7625–7651.
7. Meyers, J. P.; Darling, R. M. Model of Carbon Corrosion in PEM Fuel Cells. *J. Electrochem. Soc.* **2006**, *153*, A1432–A1442.
8. Cameron, D. S. Fuel Cells Science and Technology 2008-Scientific Advances in Fuel Cell Systems. *Platinum Met. Rev.* **2009**, *53*, 147–154.
9. Subban, C. V.; Zhou, Q.; Hu, A.; Moylan, T. E.; Wagner, F. T.; DiSalvo, F. J. Sol−Gel Synthesis, Electrochemical Characterization, and Stability Testing of $Ti_{0.7}W_{0.3}O_2$ Nanoparticles for Catalyst Support Applications in Proton-Exchange Membrane Fuel Cells. *J. Am. Chem. Soc.* **2010**, *132*, 17531–17536.
10. Gasda, M. D.; Eisman, G. A.; Gall, D. Sputter-Deposited Pt/CrN Nanoparticle PEM Fuel Cell Cathodes: Limited Proton Conductivity Through Electrode Dewetting. *J. Electrochem. Soc.* **2010**, *157*, B71–B76.
11. Zhong, H. X.; Chen, X. B.; Zhang, H. M.; Wang, M. R.; Mao, S. S. Proton Exchange Membrane Fuel Cells with Chromium Nitride Nanocrystals as Electrocatalysts. *Appl. Phys. Lett.* **2007**, 91.
12. Avasarala, B.; Murray, T.; Li, W. Z.; Haldar, P. Titanium Nitride Nanoparticles Based Electrocatalysts for Proton Exchange Membrane Fuel Cells. *J. Mater. Chem.* **2009**, *19*, 1803–1805.
13. Yang, M.; Cui, Z.; DiSalvo, F. J. Mesoporous Titanium Nitride Supported Pt Nanoparticles as High Performance Catalysts for Methanol Electrooxidation. *Phys. Chem. Chem. Phys.* **2013**, *15*, 1088–1092.
14. Cui, Z.; Burns, R. G.; DiSalvo, F. J. Mesoporous $Ti_{0.5}Nb_{0.5}N$ Ternary Nitride as a Novel Noncarbon Support for Oxygen Reduction Reaction in Acid and Alkaline Electrolytes. *Chem. Mater.* **2013**, *25*, 3782–3784.
15. Yang, M.; DiSalvo, F. J. Template Free Synthesis of Mesoporous Transition Metal Nitride Materials from Ternary Cadmium Transition Metal Oxides. *Chem. Mater.* **2012**, *24*, 4406–4409.
16. Yang, M.; Cui, Z.; DiSalvo, F. J. Mesoporous Chromium Nitride as a High Performance Non-Carbon Support for the Oxygen Reduction Reaction. *Phys. Chem. Chem. Phys.* **2013**, *15*, 7041–7044.
17. Yu, X.; Pickup, P. G. Recent Advances in Direct Formic Acid Fuel Cells (DFAFC). *J. Power Sources* **2008**, *182*, 124–132.
18. Demirci, U. B. Theoretical Means for Searching Bimetallic Alloys as Anode Electrocatalysts for Direct Liquid-Feed Fuel Cells. *J. Power Sources* **2007**, *173*, 11–18.
19. Park, S.; Xie, Y.; Weaver, M. J. Electrocatalytic Pathways on Carbon Supported Platinum Nanoparticles: Comparison of Particle-Size-Dependent Rates of Methanol, Formic Acid, and Formaldehyde Electrooxidation. *Langmuir* **2002**, *18*, 5792–5798.
20. Zhang, S.; Shao, Y. Y.; Yin, G. P.; Lin, Y. H. Electrostatic Self-Assembly of a Pt-around-Au Nanocomposite with High Activity towards Formic Acid Oxidation. *Angew. Chem., Int. Ed.* **2010**, *49*, 2211–2214.
21. Kristian, N.; Yan, Y.; Wang, X. Highly Efficient Submonolayer Pt-Decorated Au Nano-Catalysts for Formic Acid Oxidation. *Chem. Commun.* **2008**, 353–355.
22. Ji, X. L.; Lee, K. T.; Holden, R.; Zhang, L.; Zhang, J. J.; Botton, G. A.; Couillard, M.; Nazar, L. F. Nanocrystalline Intermetallics on Mesoporous Carbon for Direct Formic Acid Fuel Cell Anodes. *Nat. Chem.* **2010**, *2*, 286–293.
23. Feng, L. G.; Sun, X. J.; Liu, C. P.; Xing, W. Poisoning Effect Diminished on a Novel $PdHoO_x$/C Catalyst for the Electrooxidation of Formic Acid. *Chem. Commun.* **2012**, *48*, 419–421.
24. Wang, J. J.; Chen, Y. G.; Liu, H.; Li, R. Y.; Sun, X. L. Synthesis of Pd Nanowire Networks by a Simple Template-Free and Surfactant-Free Method and Their Application in Formic Acid Electrooxidation. *Electrochem. Commun.* **2010**, *12*, 219–222.
25. Yang, J.; Tian, C. G.; Wang, L.; Fu, H. G. An effective Strategy for Small-Sized and Highly-Dispersed Palladium Nanoparticles Supported on Graphene with Excellent Performance for Formic Acid Oxidation. *J. Mater. Chem.* **2011**, *21*, 3384–3390.
26. Bai, Z. Y.; Yang, L.; Li, L.; Lv, J.; Wang, K.; Zhang, J. A Facile Preparation of Hollow Palladium Nanosphere Catalysts for Direct Formic Acid Fuel Cell. *J. Phys. Chem. C* **2009**, *113*, 10568–10573.
27. Ha, S.; Larsen, R.; Zhu, Y.; Masel, R. I. Direct Formic Acid Fuel Cells with 600 mA cm^{-2} at 0.4 V and 22 °C. *Fuel Cells* **2004**, *4*, 337–343.
28. Yu, X. W.; Pickup, P. G. Deactivation/Reactivation of a Pd/C Catalyst in a Direct Formic Acid Fuel Cell (DFAFC): Use of Array Membrane Electrode Assemblies. *J. Power Sources* **2009**, *187*, 493–499.
29. Yu, X. W.; Pickup, P. G. Deactivation Resistant PdSb/C Catalysts for Direct Formic Acid Fuel Cells. *Electrochem. Commun.* **2010**, *12*, 800–803.
30. Wang, Y.; Sheng, Z. M.; Yang, H. B.; Jiang, S. P.; Li, C. M. Electrocatalysis of Carbon Black- or Activated Carbon Nanotubes-Supported Pd-Ag towards Methanol Oxidation in Alkaline Media. *Int. J. Hydrogen Energy* **2010**, *35*, 10087–10093.
31. Estudillo-Wong, L. A.; Vargas-Gomez, A. M.; Arce-Estrada, E. M.; Manzo-Robledo, A. TiO_2/C Composite as a Support for Pd-nanoparticles toward the Electrocatalytic Oxidation of Methanol in Alkaline Media. *Electrochim. Acta* **2013**, *112*, 164–170.
32. Wang, X. M.; Xia, Y. Y. Electrocatalytic Performance of PdCo-C Catalyst for Formic Acid Oxidation. *Electrochem. Commun.* **2008**, *10*, 1644–1646.
33. Vidal-Iglesias, F. J.; Solla-Gullon, J.; Herrero, E.; Aldaz, A.; Feliu, J. M. Pd Adatom Decorated (100) Preferentially Oriented Pt Nanoparticles for Formic Acid Electrooxidation. *Angew.Chem., Int. Ed.* **2010**, *49*, 6998–7001.
34. Zhou, W. J.; Lee, J. Y. Highly Active Core-Shell Au@Pd Catalyst for Formic Acid Electrooxidation. *Electrochem. Commun.* **2007**, *9*, 1725–1729.
35. Baldauf, M.; Kolb, D. M. Formic Acid Oxidation on Ultrathin Pd Films on Au(hkl) and Pt(hkl) Electrodes. *J. Phys. Chem.* **1996**, *100*, 11375–11381.
36. Feng, L. G.; Yan, L. A.; Cui, Z. M.; Liu, C. P.; Xing, W. High Activity of Pd-WO_3/C Catalyst as Anodic Catalyst for Direct Formic Acid Fuel Cell. *J. Power Sources* **2011**, *196*, 2469–2474.
37. Watanabe, M.; Motoo, S. Electrocatalysis by Ad-Atoms: Part III. Enhancement of the Oxidation of Carbon Monoxide on Platinum by Ruthenium Ad-Atoms. *J. Electroanal. Chem. Interfacial Electrochem.* **1975**, *60*, 275–283.
38. McBreen, J.; Mukerjee, S. *In Situ* X-Ray Absorption Studies of a Pt-Ru Electrocatalyst. *J. Electrochem. Soc.* **1995**, *142*, 3399–3404.
39. Shibata, M.; Motoo, S. Electrocatalysis by ad-atoms: Part XV. Enhancement of CO Oxidation on Platinum by the Electronegativity of Ad-Atoms. *J. Electroanal. Chem. Interfacial Electrochem.* **1985**, *194*, 261–274.
40. Pantea, D.; Darmstadt, H.; Kaliaguine, S.; Summchen, L.; Roy, C. Electrical Conductivity of Thermal Carbon

Blacks—Influence of Surface Chemistry. *Carbon* **2001**, *39*, 1147–1158.
41. Cui, Z. M.; Liu, C. P.; Liao, J. H.; Xing, W. Highly Active PtRu Catalysts Supported on Carbon Nanotubes Prepared by Modified Impregnation Method for Methanol Electro-Oxidation. *Electrochim. Acta* **2008**, *53*, 7807–7811.
42. Capon, A.; Parsons, R. The Oxidation of Formic Acid at Noble Metal Electrodes Part III. Intermediates and Mechanism on Platinum Electrodes. *J. Electroanal. Chem. Interfacial Electrochem.* **1973**, *45*, 205–231.
43. Vela, M. E.; Lezna, R. O.; De Tacconi, N. R.; Arvia, A. J.; Beden, B.; Hahn, F.; Lamy, C. EMIRS Studies of Formic Acid Electrooxidation on Pd, Au and Pd + Au Alloys: Part 1. Investigation of the Adsorbates Derived from HCOOH and NACOOH Chemisorption at Pd in Acid and Alkaline Solutions. *J. Electroanal. Chem.* **1992**, *323*, 289–302.
44. Miyake, H.; Okada, T.; Samjeske, G.; Osawa, M. Formic Acid Electrooxidation on Pd in Acidic Solutions Studied by Surface-Enhanced Infrared Absorption Spectroscopy. *Phys. Chem. Chem. Phys.* **2008**, *10*, 3662–3669.
45. Yu, X. W.; Pickup, P. G. Mechanistic Study of the Deactivation of Carbon Supported Pd During Formic Acid Oxidation. *Electrochem. Commun.* **2009**, *11*, 2012–2014.
46. Wang, Y.; Li, L.; Hu, L.; Zhuang, L.; Lu, J.; Xu, B. A Feasibility Analysis for Alkaline Membrane Direct Methanol Fuel Cell: Thermodynamic Disadvantages *versus* Kinetic Advantages. *Electrochem. Commun.* **2003**, *5*, 662–666.
47. Hammer, B.; Nørskov, J. K. Electronic Factors Determining the Reactivity of Metal Surfaces. *Surf. Sci.* **1995**, *343*, 211–220.
48. Hammer, B.; Nørskov, J. K. Theoretical Surface Science and Catalysis—Calculations and Concepts. In *Advances in Catalysis*; Bruce, C., Gates, H. K., Eds.; Academic Press: Waltham, MA, 2000; Vol. 45, pp 71–129.
49. Greeley, J.; Nørskov, J. K. A General Scheme for the Estimation of Oxygen Binding Energies on Binary Transition Metal Surface Alloys. *Surf. Sci.* **2005**, *592*, 104–111.
50. Yang, M. H.; MacLeod, M. J.; Tessier, F.; DiSalvo, F. J. Mesoporous Metal Nitride Materials Prepared from Bulk Oxides. *J. Am. Ceram. Soc.* **2012**, *95*, 3084–3089.